ACS OMEGA

Open Access



http://pubs.acs.org/journal/acsodf

Article

# Python-Based Algorithm for Calculating Physical Properties of Aqueous Mixtures Composed of Substances Not Available in Databases

Jina Lee, Se-Hee Jo, Chungyup Lee, Ji Hun Kang, Wangyun Won,* and Jun-Woo Kim*

Cite This: *ACS Omega* 2025, 10, 16683−16694

Read Online

ACCESS | Metrics & More | Article Recommendations | Supporting Information

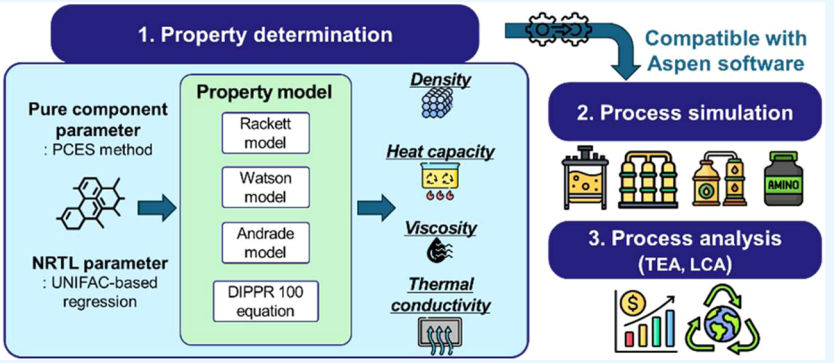


**ABSTRACT:** In this study, we developed a Python-based open-source algorithm compatible with the aqueous physical property models provided in the electrolyte templates of AspenTech software. To validate the accuracy of the model, the results obtained from the proposed algorithm were compared to experimental data for 37 binary aqueous mixture systems covering properties such as density, heat capacity, viscosity, and thermal conductivity. The input variables included results from our previous research on pure component property prediction and the nonrandom two-liquid (NRTL) model parameters based on the UNIFAC model simulations. This open-source algorithm is compatible with AspenTech software. The mean absolute percentage errors (MAPE) for density, heat capacity, viscosity, and thermal conductivity were 2.88, 0.355, 12.1, and 10.1%, respectively. In the case of density and viscosity, the actual data trends could not be accurately reflected under high-concentration conditions for certain substances. In addition, it was confirmed that inaccurate predictions of the viscosity and thermal conductivity in the commercial-scale falling-film evaporator simulation for L-valine production led to inaccurate predictions of the overall heat transfer coefficient. Therefore, caution is required when predicting missing property parameters using this approach as significant errors may occur. Nevertheless, this algorithm can provide an initial parameter value for property models that are not included in existing databases without any commercial package.

## 1. INTRODUCTION

Selecting appropriate models for calculating the physical properties of process streams, such as the density, heat capacity, viscosity, and thermal conductivity, is an essential step in process design.[1−4] Commercial software such as Aspen Plus, Aspen HYSYS, PRO/II, DynSim, and gPROMS are widely used for process modeling and simulation because they provide various property models for calculating the physical properties..[5,6] However, these software packages only provide information on the equations of the property models, and specific algorithms have not been disclosed.[7] This makes providing a clear theoretical reference or customizing the physical property models difficult. In addition, a commercial license fee must be paid to use this software, which can be a burden on individual users.

In aqueous solutions generated during the production of biobased substances such as alcohol, amino acids, and organic acids, there may exist various unfamiliar components for which property databases do not exist.[8−10] When resources are inadequate for obtaining the experimental property information, the Aspen Property Constant Estimation System (PCES) method[7] is useful. The normal boiling point,[11−14] critical properties,[11−13] acentric factor,[11−13] enthalpy of formation,[15] ideal gas heat capacity,[16] and activity coefficient[17−19] have

Received: January 15, 2025
Revised: March 31, 2025
Accepted: April 4, 2025
Published: April 15, 2025





https://doi.org/10.1021/acsomega.5c00424
*ACS Omega* 2025, 10, 16683−16694

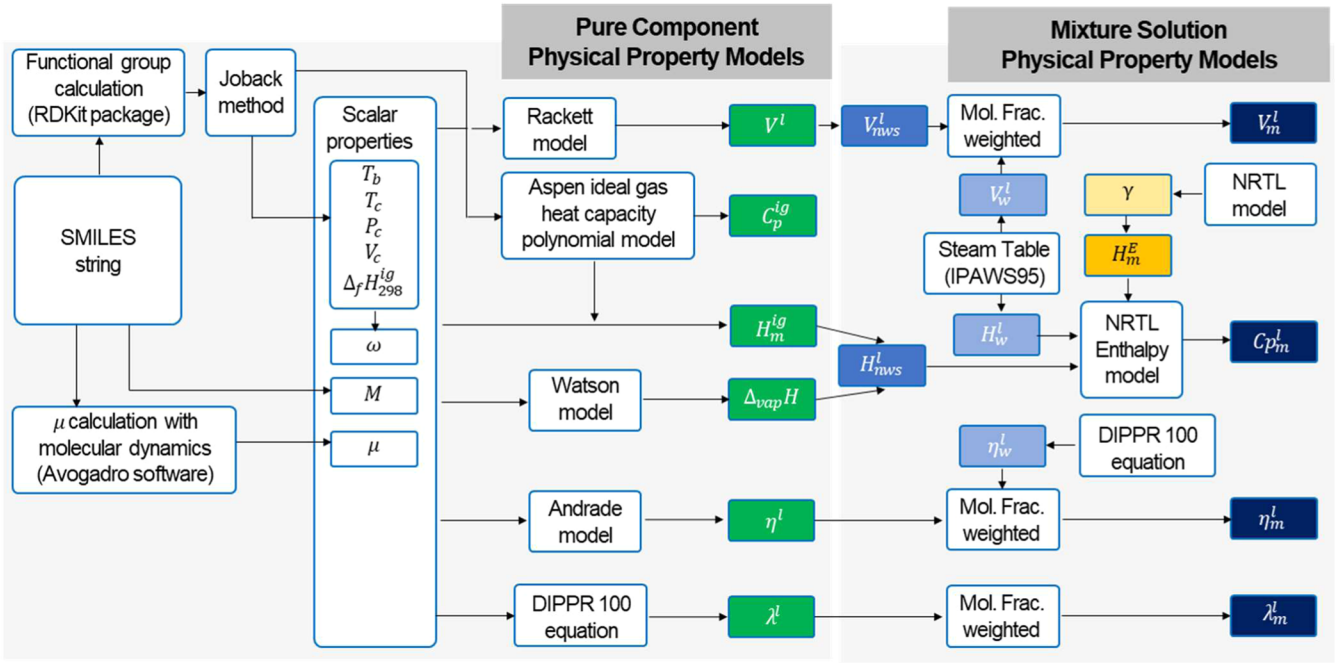


**Figure 1.** Algorithm for calculating the physical properties of mixtures. The pure component physical property calculation stage has been described in our previous study.[3]

been estimated using PCES during process optimization, technoeconomic analysis, or life cycle assessment.[20−23] In our previous study, we developed a Python-based open-source algorithm that is compatible with the PCES method for predicting the physical properties of pure substances.[3] However, because almost all biobased liquids exist in aqueous solutions,[24] it is impossible to perform process modeling and simulation using only the properties of pure substances.

In this study, we developed a Python-based open-source algorithm compatible with the aqueous physical property models provided in the electrolyte templates of the AspenTech software. To verify the accuracy of the model, the results calculated using the proposed Python-based algorithm were compared with the experimental values of 37 binary aqueous mixture systems, including the density, heat capacity, viscosity, and thermal conductivity.[1] Specifically, the 37 binary aqueous mixture systems consisted of 20 amino acids, 6 organic acids, and 11 sugar solutions. The experimental data used in this study for the aqueous solutions consisted of 2009, 1311, 1247, and 169 data points for density, heat capacity, viscosity, and thermal conductivity, respectively.

In the model used in this study, the calculation of the heat capacity of the mixture requires the parameters of the nonrandom two-liquid (NRTL) activity coefficient model.[25,26] The AspenTech software allows us to obtain NRTL model parameters by regression from the simulation results of universal quasi-chemical functional group activity coefficient (UNIFAC).[7] We also developed a Python-based open-source algorithm to estimate the NRTL model parameters from UNIFAC model simulation results with a higher accuracy than that of the AspenTech software method,[27] which was also applied in the current study.

One of the main objectives of this study is to introduce an accurate algorithm of the Aspen PCES method for calculating aqueous mixture properties to potential users of the AspenTech software. Additionally, this study aims to explain the limitations of the Aspen PCES method through a comparison between experimental data and calculated physical property results. The impact of inaccurate property models on the overall heat transfer coefficient was also examined through a simulation of the heat exchanger in a commercial falling-film evaporator.

In summary, this study introduced a comprehensive method for calculating the physical properties of aqueous solutions compatible with AspenTech software, utilizing Python-based open-source algorithms as part of an open-source initiative.[28] The predicted results were rigorously compared with a wide range of experimental data obtained from aqueous mixtures, allowing for a detailed analysis of the accuracy and potential industrial applicability of each calculated physical property. The Python-based open-source algorithms that we developed have the potential to serve as clear and standardized guidelines for the development of property models within the industrial biotechnology community. Nevertheless, the accuracy, limitations, and precautions for using the Python-based open-source algorithms based on the Aspen PCES method were discussed.

## 2. METHODS

**2.1. Chemicals.** Twenty amino acids (L-aspartic acid, L-threonine, L-serine, L-glutamic acid, glycine, L-alanine, L-cysteine, L-valine, L-methionine, L-isoleucine, L-leucine, L-tyrosine, L-phenylalanine, L-lysine, L-histidine, L-arginine, L-tryptophan, L-proline, L-asparagine, and L-glutamine), 6 organic acids (citric acid, malic acid, succinic acid, lactic acid, formic acid, and acetic acid), and 11 sugars (trehalose, arabinose, galactose, glucose, mannose, xylose, fructose, sucrose, isomaltose, cellobiose, and maltose) were investigated. The chemical formulas, chemical abstract service (CAS) numbers of these chemicals, and simplified molecular input line-entry specification (SMILES) strings are summarized in Table S1 in the Supporting Information.


https://doi.org/10.1021/acsomega.5c00424
ACS Omega 2025, 10, 16683−16694

**Table 1. Heat Exchanger Geometry and Process Conditions Used in Commercial-Scale Falling Film Evaporators for L-Valine Production**

| item | case 1 | case 2 | case 3 | case 4 |
|---|---|---|---|---|
| tube length, $L$ (mm) | 10,260 | 10,260 | 8420 | 8420 |
| effective tube length, $L_{eff}$ (mm) | 9918 | 9918 | 8139 | 8139 |
| central baffle spacing, $L_{bc}$ (mm) | 658 | 658 | 540 | 540 |
| tube sheet thickness, $L_{ts}$ (mm) | 171 | 171 | 140 | 140 |
| shell inside diameter, $D_s$ (mm) | 1710 | 1710 | 1403 | 1403 |
| shell outer tube limit, $D_{otl}$ (mm) | 1689 | 1689 | 1384 | 1384 |
| diametral bundle-shell clearance, $\Delta_b$ (mm) | 21 | 21 | 20 | 20 |
| tube outside diameter, $D_o$ (mm) | 43 | 43 | 43 | 43 |
| tube inside diameter, $D_i$ (mm) | 40 | 40 | 40 | 40 |
| tube wall thickness, $L_{tw}$ (mm) | 2 | 2 | 2 | 2 |
| tube pitch, $P_t$ (mm) | 53 | 53 | 53 | 53 |
| effective tube pitch, $P_{t,eff}$ | 53 | 53 | 53 | 53 |
| tube layout characteristic angle, $\theta_{tp}$ (deg) | 30 | 30 | 30 | 30 |
| number of tubes, $N_t$ | 861 | 861 | 580 | 580 |
| heat transfer surface area, $A$ ($m^2$) | 1146 | 1146 | 633 | 633 |
| tube-side flow rate (kg $h^{-1}$) | 195,000 | 190,000 | 115,000 | 150,000 |
| tube-side temperature (K) | 343 | 339 | 332 | 327 |
| tube-side L-valine weight fraction | 0.081 | 0.0882 | 0.104 | 0.0915 |
| shell-side flow rate (kg $h^{-1}$) | 7054 | 6783 | 6326 | 3245 |
| shell-side temperature (K) | 345 | 341 | 337 | 329 |
| shell-side Reynolds number | 172 | 157 | 204 | 93 |
| overall heat transfer coefficient, $U$ (W $m^{-2}$ $K^{-1}$) | 1638 | 1471 | 1362 | 1422 |

**2.2. Unit System.** Aspen covers a wide range of property models, and its built-in templates have different unit systems, which can lead to confusion. Because industrial bioprocesses are performed in aqueous solutions, a unit system of the Aspen electrolyte template was used in this study. Summary of the unit systems based on the property models and Aspen models was summarized in our previous study.[3]

**2.3. Algorithm.** The algorithm developed in this study for calculating the mixture properties uses the property values of the pure components and NRTL parameters. The results of our previous research on pure component property prediction[3] and the NRTL model parameters based on the UNIFAC model simulation results[27] were used as inputs. As shown in Figure 1, the molar volume, heat capacity, viscosity, and thermal conductivity of the aqueous mixtures were calculated by using various mixing rule models. The detailed models for each property are described in Sections 2.3 to 2.6. The models in this study do not provide mixture property predictions for ionic species. The proposed algorithm is designed specifically for molecular species.

**2.4. Density Model.** The molar density is the reciprocal of the molar volume. Using the AspenTech software with the electrolyte template, the molar volume of the solution can be calculated using the following equation

$$V_{sol} = x_s V_s + x_e V_e \quad (1)$$

where $x$ and $V$ denote the mole fraction and molar volume, respectively. sol, s, and e denote the solution, solvent, and electrolyte, respectively. Because, in this study, we assumed that there were no electrolytes in the binary aqueous solutions, the molar volume of the solvent, $V_s$, was considered to be the same as the molar volume of the solution, $V_{sol}$.

The molar volume of solvent can be calculated by following equation

$$V_s = x_w V_w + x_{nws} V_{nws} \quad (2)$$

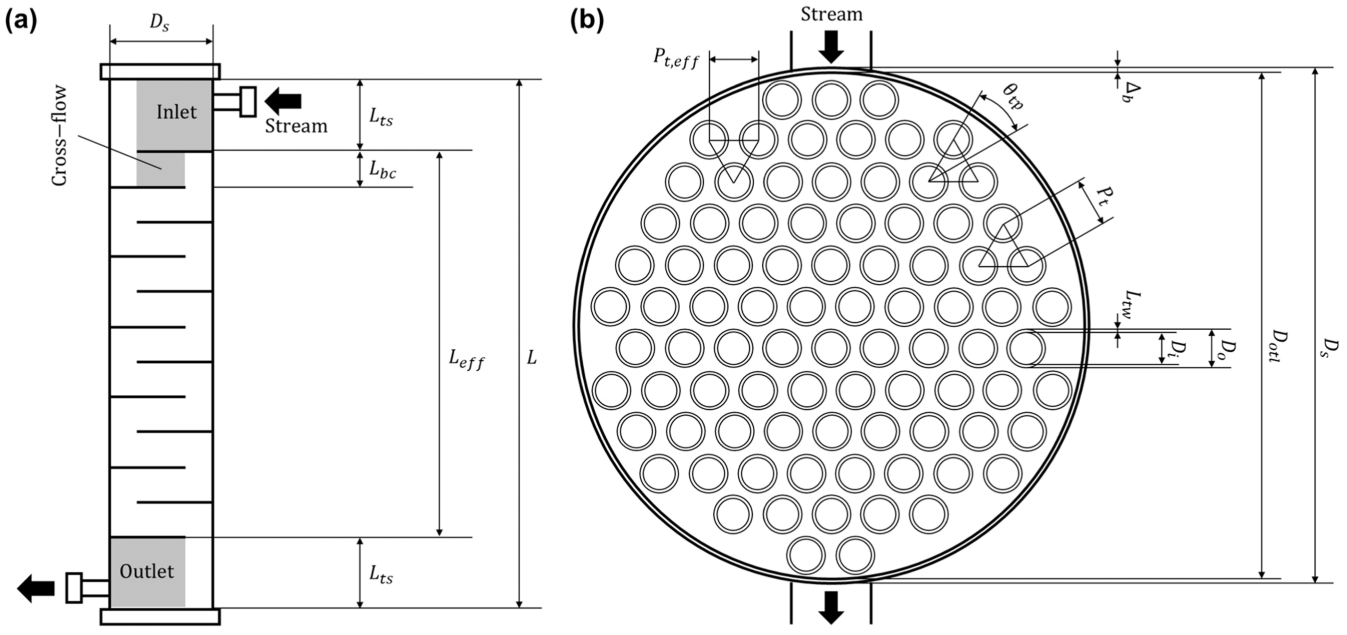


**Figure 2.** Schematics of the heat exchanger geometry for the shell side (a) and the tube side (b).



https://doi.org/10.1021/acsomega.5c00424
ACS Omega 2025, 10, 16683−16694

$$x_{nws} = \sum_{m \neq w} x_m \tag{3}$$

where w and nws denote aqueous and nonwater solvent, respectively. m indicates the molecular species. The term "nonwater solvent" is used in AspenTech software and refers to molecular species excluding water. The term "molecular species" is used in AspenTech software and refers to substances excluding ionic species. The molar volume of pure water was obtained using the IAPWS-95 steam tables provided by the International Association for the Properties of Water and Steam.[29] The modified Rackett model was used to simulate the molar volume of nonwater solvent, $V_{nws}$.[30]

$$V_{nws} = \frac{RT_{c,nws}(Z_{nws}^{RA})^{1+(1-T_{r,nws})^{2/7}}}{P_{c,nws}} \tag{4}$$

$$T_{c,nws} = \sum_{m \neq w} \sum_{n \neq w} x_m x_n V_{c,m} V_{c,n} (T_{c,m} T_{c,n})^{1/2} \frac{1 - k_{V,m,n}}{(V_{c,nws})^2} \tag{5}$$

$$k_{V,m,n} = 1 - \frac{8(V_{c,m} V_{c,n})^{1/2}}{(V_{c,m}{}^{1/3} + V_{c,n}{}^{1/3})^3} \tag{6}$$

$$\frac{T_{c,nws}}{P_{c,nws}} = \sum_{m \neq w} x_m \frac{T_{c,m}}{P_{c,m}} \tag{7}$$

$$Z_{nws}^{RA} = \sum_{m \neq w} x_m Z_m^{RA} \tag{8}$$

$$V_{c,nws} = \sum_{m \neq w} x_m V_{c,m} \tag{9}$$

$$T_{r,nws} = \frac{T}{T_{c,nws}} \tag{10}$$

where $R$, $T$, $T_c$, $P_c$, $V_c$, $T_r$, $Z^{RA}$, and $k^V$ are the gas constant, temperature, critical temperature, critical pressure, critical volume, reduced temperature, Rackett parameter, and molar volume mixing rule parameter, respectively. Both m and n indicate the molecular species. $T_c$, $P_c$, $V_c$, and $Z^{RA}$ were calculated using an algorithm described in a previous study.[3] In AspenTech software, user-defined $k_V$ values can be chosen. However, if no specific values are chosen, then the default values are set, as shown in eq 6. The default $k_V$ values were also used in this study. Both $k_{V,i,i}$ and $k_{V,j,j}$ are zero.

**2.5. Heat Capacity Model.** The heat capacity at constant pressure of an aqueous solution, $C_{p,sol}$, in cal mol$^{-1}$ K$^{-1}$ can be calculated using eq 11, for infinitesimal changes of temperature.

$$C_{p,sol} = \frac{dH_{sol}}{dT} (\text{for constant pressure}) \tag{11}$$

In addition, using AspenTech software with the electrolyte template, the molar enthalpy of the solution was calculated using the following equation

$$H_{sol} = x_w H_w + \sum_{m \neq w} x_m H_m + \sum_i x_i H_i^{\infty} + H^E \tag{12}$$

where $H$ denotes the molar enthalpy. The subscripts $m$ and $i$ denote the molecular species and the number of ionic species, respectively. The superscripts $\infty$ and $E$ denote the aqueous infinite dilution property and excess property, respectively. Because, in this study, we assume that there are no electrolytes in the binary aqueous solutions, the third term in eq 12 is negligible. The molar enthalpy of water $H_w$ was obtained using the IAPWS-95 steam tables.[29] The molar enthalpy of the molecular species $H_m$ was calculated using an algorithm developed in our previous study.[3] The excess molar enthalpy $H^E$ of the molecular species can be obtained using the following equation[31]

$$H^E = -RT^2 \left( \sum_m x_m \frac{d \ln \gamma_m}{dT} \right) (\text{for molecular species}) \tag{13}$$

where $\gamma$ is the activity coefficient. $d \ln \gamma_m / dT$ was obtained by numerical central differentiation with $1 \times 10^{-3}$ $dT$. $\gamma$ is calculated using the NRTL activity coefficient model.[32,33] The NRTL model parameters were obtained using an algorithm from our previous study,[27] in which these parameters were estimated from the results of the UNIFAC model.[34]

**2.6. Viscosity Model.** Using the AspenTech software with the electrolyte template, the viscosity of the solution can be calculated using the following equation

$$\eta_{sol} = \eta_s \left( 1 + \sum_{ca} \Delta \eta_{ca} \right) \tag{14}$$

where $\eta$ is viscosity. ca denotes the apparent electrolyte. $\Delta \eta_{ca}$ is a contribution to the viscosity correlation due to the apparent electrolyte ca. Because we assume that there are no electrolytes in the binary aqueous solutions in this study, the viscosity of the solvent, $\eta_s$, can be considered the same as the viscosity of the solution, $\eta_{sol}$. The solvent viscosity was calculated using the following equation

$$\ln \eta_s = \sum_m x_m \ln \eta_m + \sum_{i=1}^{m} \sum_{j=i+1}^{m} (k_{\eta,i,j} x_i x_j + l_{\eta,i,j} x_i^2 x_j^2) \tag{15}$$

$$k_{\eta,i,j} = k_{\eta,1,i,j} + \frac{k_{\eta,2,i,j}}{T} \tag{16}$$

$$l_{\eta,i,j} = l_{\eta,1,i,j} + \frac{l_{\eta,2,i,j}}{T} \tag{17}$$

where $k_\eta$ and $l_\eta$ are the viscosity mixing rule parameters. Both $i$ and $j$ denote the molecular species. In this study, the values for the viscosity mixing rule parameters $k_{\eta,1,i,j}$, $k_{\eta,2,i,j}$, $l_{\eta,1,i,j}$, and $l_{\eta,2,i,j}$ were set to zero, which is the default value in AspenTech software. The viscosity of the molecular species, $\eta_m$, except for that of water, was calculated using the algorithm from our previous study.[3] The viscosity of pure water, $\eta_w$, was calculated using the Design Institute for Physical Properties (DIPPR) equation 101, with the parameters implemented in the AspenTech software database as follow

$$\ln \eta_w = -45.93524472 + \frac{3703.6}{T} + 5.866 \ln T - 5.879 \times 10^{-29} T^{10} \tag{18}$$

This DIPPR equation 101 model for pure water viscosity is the default option of the electrolyte template in AspenTech software. The range of the temperature in eq 18 is from 273.16 to 646.15 K, which is also the range implemented in the AspenTech software database. In eq 18, the units of $\eta_w$ and $T$ are cP and K, respectively.



https://doi.org/10.1021/acsomega.5c00424
ACS Omega 2025, 10, 16683−16694

**2.7. Thermal Conductivity Model.** Using the AspenTech software with the electrolyte template, the thermal conductivity of the solution can be calculated using the following equation

$$\lambda_{sol} = \left(\lambda_s(T = 293K) + \sum_{ca}(a_c + a_a)\frac{x_{ca}^{app}}{V_{sol}}\right)\frac{\lambda_s(T)}{\lambda_s(T = 293\ K)} \quad (19)$$

where $\lambda$ is the thermal conductivity. $a_c$ and $a_a$ are the Riedel ionic coefficients of cation $c$ and anion a, respectively. $x_{ca}^{app}$ is the mole fraction of the apparent electrolyte $ca$. Because we assume that there are no electrolytes in the binary aqueous solutions in this study, the thermal conductivity of the solvent, $\lambda_s$, can be considered to be the same as the thermal conductivity of the solution, $\lambda_{sol}$. The thermal conductivity of the solvent was calculated using the following equation

$$(\lambda_s)^{k_\lambda} = \sum_m w_m(\lambda_m)^{k_\lambda} \quad (20)$$

where $w$ denotes the weight fraction. $k_\lambda$ is the thermal conductivity mixing rule parameter. In this study, $k_\lambda$ was set to −2, which is the default value in AspenTech software. The thermal conductivity of the molecular species, $\lambda_m$, except for that of water, was calculated using the algorithm from our previous study.[3] The thermal conductivity of pure water, $\lambda_w$, is calculated using the DIPPR equation 100, with the parameters implemented in the AspenTech software database as follows

$$\lambda_w = 0.48765298680 + 0.00148670798T - 5.6345688 \times 10^{-6}T^2 + 1.60017197 \times 10^{-9}T^3 \quad (21)$$

This DIPPR equation 100 model for pure water thermal conductivity is the default option of the electrolyte template in AspenTech software. The temperature range in eq 21 is from 0.01 to 360 °C, which is also the range implemented in the AspenTech software database. In eq 21, the units of $\lambda_w$ and $T$ are kcal m $hr^{-1}$ $m^{-2}$ °C $^{-1}$ and °C, respectively.

**2.8. Python-Based Algorithm Code.** In this study, a Python-based algorithm code was developed to calculate the physical properties of the mixtures. The pure component properties and NRTL activity coefficient parameters were calculated and used based on an algorithm developed in our previous study.[3,27] All of the algorithms introduced in this study were developed in Python, and the source codes are provided in the Supporting Information.

**2.9. Simulation of Heat Exchanger in Falling Film Evaporator.** Falling-film evaporators are commonly used in amino acid production processes to remove water.[35−37] Because the simulation of a heat exchanger in a falling-film evaporator requires properties such as density, heat capacity, viscosity, and thermal conductivity, it serves as an appropriate example for the application of aqueous mixture property models. The tube-side heat transfer coefficient $h_t$ is expressed as follows[38]

$$h_t = 0.01\left(\frac{C_{p,t}\eta_t Re_t}{\lambda_t}\right)^{1/3}\left(\frac{\lambda_t^3\rho_t^2 g}{\eta_f^2}\right)^{1/3} \quad (22)$$

where $\rho$, $Re$, and $g$ represent the density, Reynolds number, and gravitational acceleration, respectively. The subscripts t and f denote the tube side and film, respectively. The film viscosity was calculated using the average viscosity of the tube-side and wall temperatures. The wall temperature was calculated as the average of the shell- and tube-side temperatures.

Vapor condensation occurs on the shell side. The shell side of the falling film evaporator is typically designed for a laminar wavy regime ($30 < Re_s \leq 1600$). The shell side heat transfer coefficient $h_s$ for the laminar wavy regime is expressed as follows[39]

$$h_s = \frac{Re_s\left(\frac{\lambda_{s,l}^3\rho_{s,l}(\rho_{s,l} - \rho_{s,v})g}{\eta_{s,l}^2}\right)^{1/3}}{1.08Re_s^{1.22} - 5.2} \quad (23)$$

where the subscripts s, l, and v denote shell side, liquid, and vapor.

The overall heat transfer coefficient, $U$, is calculated using the following equations[38,39]

$$U = \frac{1}{\frac{1}{h_s} + \frac{1}{h_t}\frac{D_o}{D_i} + R_{tw} + R_{F,s} + R_{F,t}} \quad (24)$$

$$R_{tw} = \frac{D_o}{2\lambda_{tw}}\ln\left(\frac{D_o}{D_i}\right) \quad (25)$$

where $D_o$ and $D_i$ represent the diameters of the outer and inner tubes, respectively. $R_{tw}$ is the tube wall resistance. $\lambda_{tw}$ is the thermal conductivity of the tube wall, which is assumed to be SUS316 and is set to 0.6490 W $m^{-1}$ $K^{-1}$. $R_F$ denotes the fouling factor. Because the tube side undergoes frequent cleaning-in-pipe operations, $R_{F,t}$ was assumed to be 0 $m^2$ K $W^{1-}$. For the vapor and condensate flows on the shell side, $R_{F,s}$ was assumed to be 0.0002 $m^2$ K $W^{1-}$. This value aligns with the typical rule of thumb used by the CJ Cheil Jedang Co. (South Korea).

Table 1 summarizes the process conditions and measured values of the overall heat transfer coefficient for commercial-scale L-valine production. Overall heat transfer coefficient was obtained by dividing the measured vapor flow rate by both the heat transfer surface area and the measured temperature difference between shell and tube sides. Figure 2 illustrates the geometric structures of the shell and tube sides. In this study, the accuracy of physical property models and their impact on heat exchanger simulations were analyzed by comparing the actual measurements and simulation results.

## 3. RESULTS AND DISCUSSION

**3.1. Density.** The experimental values for 20 amino acids, 6 organic acids, and 11 sugars in aqueous solutions, totaling 2009 data points, were compared with the results obtained from the Python-based algorithm, as presented in Table 2. The mean absolute percentage error (MAPE), as shown in eq 26, is applied to measure prediction accuracy.

$$\text{MAPE} = 100\frac{1}{n}\sum_{i=1}^{n}\left|\frac{M_i - C_i}{M_i}\right| \quad (26)$$

where $M$ and $C$ are measured and calculated values, respectively, with the number of data points, $n$. MAPEs for the density of amino acids, organic acids, and sugars in aqueous solutions were 0.189, 5.43, and 5.05%, respectively. Figure 3 shows that the accuracy for amino acids is high,


https://doi.org/10.1021/acsomega.5c00424
ACS Omega 2025, 10, 16683−16694

**Table 2. MAPE Results of the Density of Amino Acids, Organic Acids, and Sugars in Aqueous Solutions**

| chemical | data points | MAPE (%) | temperature range (°C) | solute mass fraction range |
|---|---|---|---|---|
| L-aspartic acid | 39 | 0.0604 | 15−55 | 0.255−0.496 |
| L-threonine | 52 | 0.259 | 15−55 | 0.104−1.97 |
| L-serine | 54 | 0.330 | 15−55 | 0.203−3.17 |
| L-glutamic acid | 40 | 0.143 | 15−55 | 0.488−0.894 |
| glycine | 49 | 0.344 | 15−55 | 0.0840−3.38 |
| L-alanine | 43 | 0.106 | 15−55 | 0.207−2.43 |
| L-cysteine | 5 | 1.10 | 25 | 6.84−14.6 |
| L-valine | 65 | 0.0349 | 15−55 | 0.220−3.85 |
| L-methionine | 48 | 0.420 | 20−45 | 0.372−2.90 |
| L-isoleucine | 45 | 0.111 | 15−55 | 0.471−3.14 |
| L-leucine | 28 | 0.100 | 15−55 | 0.273−2.230 |
| L-tyrosine | 120 | 0.00802 | 15−55 | 0.0264−0.0445 |
| L-phenylalanine | 53 | 0.184 | 15−55 | 0.525−2.16 |
| L-lysine | 10 | 1.17 | 20−40 | 5.00−10.0 |
| L-histidine | 40 | 0.398 | 15−55 | 0.327−3.75 |
| L-arginine | 27 | 0.536 | 15−55 | 0.513−4.80 |
| L-tryptophan | 71 | 0.132 | 15−55 | 0.165−0.906 |
| L-proline | 53 | 0.0177 | 15−55 | 0.0600−7.44 |
| L-asparagine | 47 | 0.163 | 15−55 | 0.181−2.25 |
| L-glutamine | 41 | 0.200 | 15−55 | 0.0815−1.98 |
| citric acid | 36 | 19.8 | 25−40 | 0.0643−0.450 |
| malic acid | 19 | 5.29 | 10−60 | 0.00200−0.442 |
| succinic acid | 16 | 1.11 | 25 | 0.00717−0.0680 |
| lactic acid | 24 | 7.51 | 20−80 | 0.0916−0.455 |
| formic acid | 130 | 6.43 | 15−55 | 0.00179−0.479 |
| acetic acid | 225 | 2.65 | 5−85 | 0.00127−0.497 |
| trehalose | 6 | 0.603 | 25 | 0.0350−0.0735 |
| arabinose | 6 | 1.50 | 25 | 0.00752−0.0433 |
| galactose | 6 | 1.83 | 25 | 0.00889−0.0512 |
| glucose | 117 | 7.61 | 15−40 | 0.000449−0.423 |
| mannose | 90 | 6.24 | 15−25 | 0.000435−0.256 |
| xylose | 5 | 1.75 | 25 | 0.0148−0.0433 |
| fructose | 117 | 10.1 | 15−40 | 0.000470−0.423 |
| sucrose | 73 | 4.98 | 15−55 | 0.0168−0.461 |
| isomaltose | 132 | 0.792 | 5−95 | 0.0102−0.158 |
| cellobiose | 77 | 0.541 | 5−95 | 0.0109−0.0955 |
| maltose | 132 | 0.792 | 5−95 | 0.0102−0.158 |

whereas the errors observed for organic acids and sugars in aqueous solutions are relatively large.

To analyze the sources of error, the correlation coefficient of MAPE was calculated. The analysis revealed that the mass fraction of the nonsolvent water exhibited a high correlation coefficient of 0.820, and $Z^{RA}$ had the second highest correlation coefficient of 0.365. The density model for the aqueous mixtures follows the density of water at low concentrations. Consequently, at higher concentrations, the model tends to exhibit amplified errors, leading to increased discrepancies. In practice, the organic acids and sugars, which had relatively higher errors, were compared to experimental values within higher concentration ranges, in contrast to the amino acids. $Z^{RA}$ is a parameter of the Rackett model applied to the molar volume model for the pure component. The parameter estimated by Gunn and Yamada is based on experimental data for 26 nonpolar substances,[40] may introduce errors for the substances used in this study. In particular, the densities of formic acid and acetic acid exhibited a decreasing trend with increasing concentration, which contrasts with the behavior

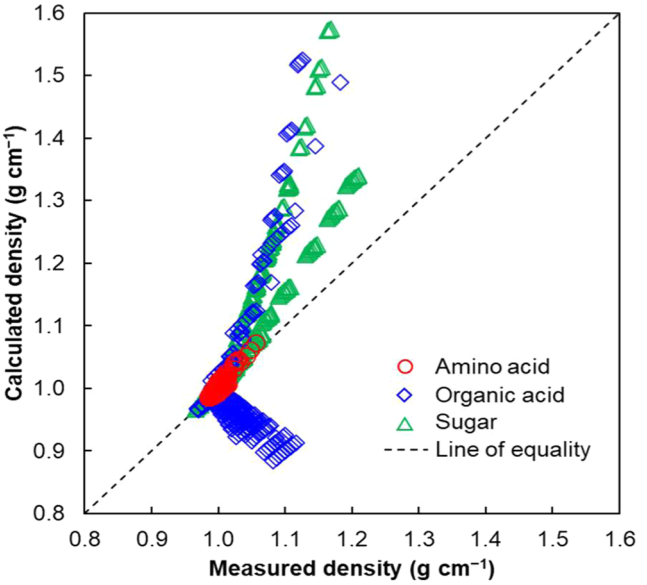


**Figure 3.** Density of amino acids, organic acids, and sugars in aqueous solutions with experimental and calculated results.

observed for other substances. This discrepancy arises because the empirically applied $Z^{RA}$ values exhibited limited accuracy.

Unlike in eq 1, our previous study reported that by not treating water as a separate solvent term, introducing a mixing parameter between water and another substance, and fitting the parameters to actual data, a good fit could be achieved.[1] However, in the Aspen electrolyte template, the solubility of water is fixed, which prevents the introduction of a mixing parameter. In this case, to improve accuracy in Aspen, one could either use a different template that does not fix the density of water as a solvent, such as a chemical template, or modify $Z^{RA}$.

Although they require high computational performance and user expertise, molecular dynamics simulations are a good alternative for calculating the density of aqueous solutions. In molecular dynamics simulations of aqueous solutions of 20 amino acids using the GROMOS, OPLS-AA, and CHARMM force fields, the percentage absolute residuals were reported to be within 0.5%.[41] In the simulations of the densities of high-concentration (10 to 50 wt %) aqueous sucrose solutions using the OPLS-AA force field, the percentage of absolute residuals was reported to be within 3%.[42]

**3.2. Heat Capacity.** The experimental values for 20 amino acids, 6 organic acids, and 11 sugars in aqueous solutions, totaling 1311 data points, were compared with the results obtained from the Python-based algorithm, as presented in Table 3. MAPEs for the heat capacity for amino acids, organic acids, and sugars in aqueous solutions were 0.157, 0.544, and 1.81%, respectively. As shown in Figure 4, the overall accuracy was high, with an average absolute residual percentage of approximately 0.355%.

The cases in which crossovers occurred within the temperature range of the heat capacity measurements, such as those of lysine and threonine, were difficult to model using the proposed algorithm, as shown in Figure 5. The activity coefficient influences the rate of change in the heat capacity with respect to the model fraction of amino acids in aqueous solutions. Previous research has confirmed that the NRTL model accurately represents this gradient.[2] Similarly, this study


https://doi.org/10.1021/acsomega.5c00424
ACS Omega 2025, 10, 16683−16694

Table 3. MAPE Results of the Heat Capacity of Amino Acids, Organic Acids, and Sugars in Aqueous Solutions

| chemical | data points | MAPE (%) | temperature range (°C) | solute mass fraction range |
|---|---|---|---|---|
| L-aspartic acid | 39 | 0.0813 | 15−55 | 0.00255−0.00496 |
| L-threonine | 50 | 0.0804 | 15−55 | 0.00104−0.0197 |
| L-serine | 45 | 0.406 | 15−55 | 0.00203−0.0317 |
| L-glutamic acid | 40 | 0.0852 | 15−55 | 0.00488−0.00894 |
| glycine | 45 | 0.682 | 15−55 | 0.000840−0.0338 |
| L-alanine | 42 | 0.169 | 15−55 | 0.00207−0.0243 |
| L-cysteine | 20 | 0.137 | 5−75 | 0.0120−0.0571 |
| L-valine | 64 | 0.172 | 15−55 | 0.00220−0.0385 |
| L-methionine | 75 | 0.0446 | 15−55 | 0.00644−0.0152 |
| L-isoleucine | 44 | 0.343 | 15−55 | 0.00471−0.0314 |
| L-leucine | 28 | 0.281 | 15−55 | 0.00273−0.0223 |
| L-tyrosine | 97 | 0.0180 | 15−25 | 0.000264−0.000445 |
| L-phenylalanine | 53 | 0.138 | 15−55 | 0.00525−0.0216 |
| L-lysine | 40 | 0.442 | 15−55 | 0.00562−0.0286 |
| L-histidine | 39 | 0.102 | 15−55 | 0.00327−0.0375 |
| L-arginine | 28 | 0.0622 | 15−55 | 0.00513−0.0921 |
| L-tryptophan | 71 | 0.0178 | 15−55 | 0.00165−0.00906 |
| L-proline | 100 | 0.113 | 15−55 | 0.000600−0.0744 |
| L-asparagine | 39 | 0.241 | 15−55 | 0.00181−0.0196 |
| L-glutamine | 39 | 0.178 | 15−55 | 0.000815−0.0198 |
| citric acid | 5 | 2.07 | 0 | 0.0201−0.103 |
| malic acid | 5 | 3.60 | 0 | 0.0202−0.104 |
| succinic acid | 15 | 0.813 | 30−100 | 0.0280−0.0426 |
| lactic acid | 1 | 5.25 | 25 | 1.00 |
| formic acid | 44 | 0.644 | 0−100 | 0.0221−0.116 |
| acetic acid | 186 | 0.350 | 0−100 | 0.00193−0.153 |
| trehalose | 5 | 0.255 | 25 | 0.0200−0.100 |
| arabinose | 10 | 0.380 | 30 | 0.0291−0.139 |
| galactose | 7 | 2.08 | 30 | 0.0591−0.165 |
| glucose | 22 | 1.51 | 25 | 0.0348−0.260 |
| mannose | 7 | 2.02 | 30 | 0.0594−0.171 |
| xylose | 10 | 0.583 | 30 | 0.0298−0.142 |
| fructose | 12 | 1.67 | 30 | 0.0365−0.165 |
| sucrose | 12 | 5.61 | 10−60 | 0.105−0.398 |
| isomaltose | 7 | 0.917 | 30 | 0.0781−0.156 |
| cellobiose | 5 | 0.277 | 25 | 0.0200−0.100 |
| maltose | 7 | 0.917 | 30 | 0.0781−0.156 |

achieved high accuracy using the NRTL model; however, modeling the phenomenon of crossover in the considered temperature range for some amino acids remains challenging. In cases requiring a highly accurate property design, the regression of NRTL parameters based on experimental data is necessary.

**3.3. Viscosity.** The experimental values for 20 amino acids, 6 organic acids, and 11 sugars in aqueous solutions, totaling 1247 data points, were compared with the results obtained from the Python-based algorithm, as presented in Table 4. MAPEs for the viscosities of the amino acids, organic acids, and sugars in aqueous solutions were 5.81, 30.0, and 61.8%, respectively. Figure 6 indicates that the accuracy of the viscosity predictions is generally not high.

As shown in Figure 6, the calculated values were generally lower than the measured values. This indicates that the rate of change in the calculated values with respect to the mass fraction was consistently lower than that in the measured values. In this study, the Letsou−Stiel model was applied to obtain the viscosity of the pure components.[43] Because the Letsou−Stiel model was developed based on hydrocarbons

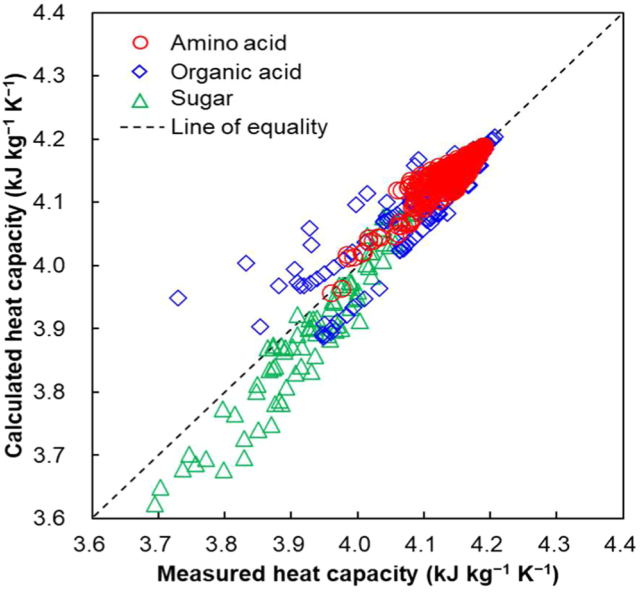


Figure 4. Heat capacity of amino acids, organic acids, and sugars in aqueous solutions with experimental and calculated results.

that exhibit lower interactions than other substances, it is expected that the model does not adequately account for the characteristics of bioderived substances with strong interactions. To address these discrepancies, a mixing rule parameter should be introduced in the model. Currently, the value of this term is set to the default value of zero in the Aspen electrolyte template. However, it is necessary to introduce substance-specific values based on experimental data to improve the accuracy of predictions.

The simulation of the viscosity of aqueous solutions remains challenging even with sophisticated molecular dynamics simulations. In the viscosity simulation of aqueous solutions of glycine, valine, phenylalanine, and asparagine using the OPLS-AA, GROMOS, Amber, and CHARMM force fields, the absolute percentage error residuals were reported to be as high as 80%.[44] In the simulations of aqueous sucrose solutions using the OPLS-AA force field, the absolute percentage error residuals were reported to be within 40%.[42] Nevertheless, these results are more accurate compared with those obtained using the Aspen PCES method.

**3.4. Thermal Conductivity.** The experimental values for 20 amino acids, totaling 169 data points, were compared with the results obtained by using the Python-based algorithm, as presented in Table 5. The thermal conductivity data for the organic acid and sugar aqueous solutions were not obtained. MAPE for the thermal conductivity of the amino acids in aqueous solutions was 22.1%. Figure 7 suggests that the accuracy of the thermal conductivity predictions for the amino acid solutions is low. The correlation coefficient of MAPE was calculated. The analysis revealed that the mass fraction of nonsolvent water exhibited a high correlation coefficient of 0.789. The results of the thermal conductivity model for aqueous mixtures followed the thermal conductivity of water at low concentrations. At higher concentrations, the model tends to exhibit amplified errors, leading to increased discrepancies.

In eq 20, the mixing rule parameter $k_\lambda$ is fixed at −2, which restricts the ability to apply substance-specific values to AspenTech software. This algorithm follows the Aspen electrolyte template to establish a basis for predicting the


https://doi.org/10.1021/acsomega.5c00424
ACS Omega 2025, 10, 16683−16694

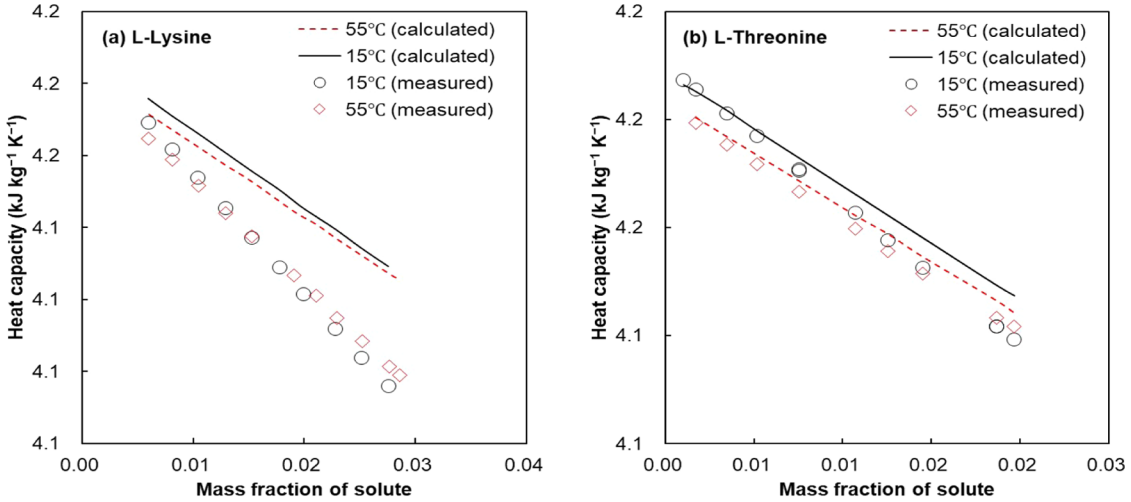


**Figure 5.** Heat capacities of L-lysine (a) and L-threonine (b) in aqueous solutions with experimental and calculated results.

**Table 4. MAPE Results of the Viscosity of Amino Acids, Organic Acids, and Sugars in Aqueous Solutions**

| chemical | data points | MAPE (%) | temperature range (°C) | solute mass fraction range |
|---|---|---|---|---|
| L-aspartic acid | 24 | 2.10 | 15−45 | 0.000688−0.00200 |
| L-threonine | 8 | 8.02 | 25 | 0.00979−0.0733 |
| L-serine | 27 | 2.67 | 5−35 | 0.00307−0.0300 |
| L-glutamic acid | 24 | 2.03 | 15−45 | 0.00162−0.0044 |
| glycine | 40 | 4.74 | 15−45 | 0.000905−0.0580 |
| L-alanine | 40 | 9.05 | 15−45 | 0.000836−0.0664 |
| L-cysteine | 25 | 40.9 | 30−50 | 0.0475−0.276 |
| L-valine | 36 | 10.6 | 15−45 | 0.000650−0.0449 |
| L-methionine | 48 | 1.86 | 20−45 | 0.00372−0.0290 |
| L-isoleucine | 42 | 7.43 | 20−45 | 0.000−0.0193 |
| L-leucine | 7 | 0.994 | 25 | 0.00257−0.0106 |
| L-tyrosine | 20 | 0.9435 | 25−40 | 0.00181−0.00906 |
| L-phenylalanine | 18 | 1.65 | 25−40 | 0.00329−0.0194 |
| L-lysine | 30 | 3.20 | 30−50 | 0.00420−0.0209 |
| L-histidine | 20 | 0.988 | 25−40 | 0.00309−0.0153 |
| L-arginine | 13 | 14.5 | 25 | 0.000−0.123 |
| L-tryptophan | 48 | 3.83 | 25−50 | 0.000−0.00756 |
| L-proline | 10 | 50.2 | 25 | 0.000−0.353 |
| L-asparagine | 5 | 0.407 | 25 | 0.00264−0.0130 |
| L-glutamine | 4 | 0.345 | 25 | 0.00291−0.0116 |
| citric acid | 28 | 27.5 | 20−50 | 0.0300−0.210 |
| malic acid | 2 | 40.8 | 20 | 0.000−0.500 |
| succinic acid | 14 | 3.15 | 35 | 0.000681−0.0554 |
| lactic acid | 42 | 61.9 | 25−80 | 0.0916−0.853 |
| formic acid | 153 | 27.4 | 15−55 | 0.00230−1.00 |
| acetic acid | 169 | 27.8 | 15−55 | 0.000700−0.691 |
| trehalose | 21 | 1.39 | 20−34 | 0.000−0.450 |
| arabinose | 15 | 20.5 | 35−50 | 0.0292−0.131 |
| galactose | 6 | 61.8 | 25 | 0.0336−0.151 |
| glucose | 79 | 51.8 | 0−85 | 0.100−0.600 |
| mannose | 20 | 37.7 | 15−45 | 0.0801−0.410 |
| xylose | 6 | 18.3 | 25 | 0.0282−0.132 |
| fructose | 112 | 52.1 | 0−85 | 0.000−0.600 |
| sucrose | 112 | 46.6 | 0−85 | 0.000−0.600 |
| isomaltose | 15 | 32.9 | 35−50 | 0.0641−0.255 |
| cellobiose | 20 | 51.9 | 15−45 | 0.139−0.529 |
| maltose | 15 | 32.9 | 35−50 | 0.0641−0.255 |

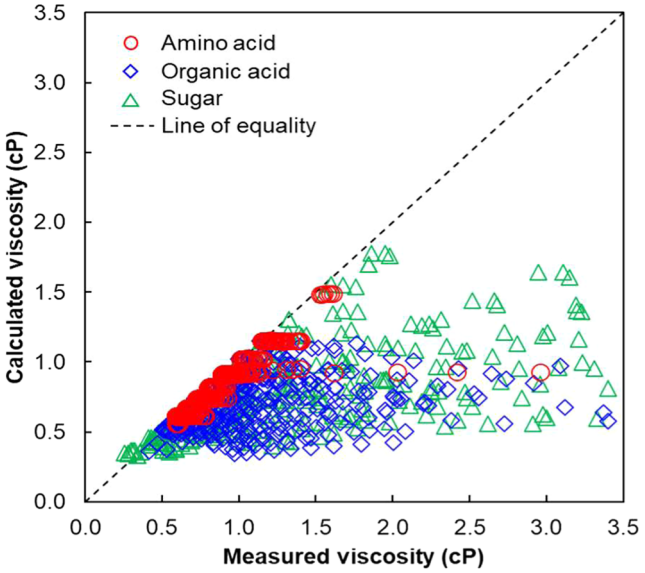


**Figure 6.** Viscosity of amino acids, organic acids, and sugars in aqueous solutions with experimental and calculated results.

initial properties of the mixed solutions. However, to obtain accurate values rather than merely initial estimates, it is imperative to introduce substance-specific mixing rule parameters derived from experimental data. This approach was successfully implemented in our previous research, where we confirmed that MAPE could be enhanced to within 2%.[1]

**3.5. Effect of Mass Fraction and Temperature on Error.** The correlation coefficients between the solute mass fraction and MAPE for the density, heat capacity, viscosity, and thermal conductivity data were 0.672, 0.618, 0.799, and 0.623, respectively. Because an accurate model was applied to predict pure water properties, it is expected that a high accuracy is observed at low solute mass fractions. However, as the solute mass fraction increases, the impact of the inaccurately predicted pure properties of the solute becomes more significant. As a result, the MAPEs increase with increasing the solute mass fraction. The correlation coefficients between the temperature and MAPE for the density, heat capacity, viscosity, and thermal conductivity data were 0.0105,


https://doi.org/10.1021/acsomega.5c00424
ACS Omega 2025, 10, 16683−16694

Table 5. MAPE Results for the Viscosity of Amino Acids in Aqueous Solutions

| chemical | data points | MAPE (%) | temperature range (°C) | solute mass fraction range |
|---|---|---|---|---|
| L-aspartic acid | 5 | 6.39 | 30 | 0.000950−0.00364 |
| L-threonine | 17 | 13.1 | 25−60 | 0.0196−0.0782 |
| L-serine | 5 | 3.88 | 30 | 0.00930−0.0347 |
| L-glutamic acid | 4 | 0.252 | 30 | 0.00184−0.00405 |
| glycine | 5 | 20.3 | 30 | 0.440−0.175 |
| L-alanine | 5 | 20.0 | 30 | 0.0333−0.126 |
| L-cysteine | 4 | 2.87 | 30 | 0.00183−0.00744 |
| L-valine | 12 | 16.3 | 30−60 | 0.0125−0.0500 |
| L-methionine | 12 | 21.9 | 25−60 | 0.0130−0.0686 |
| L-isoleucine | 16 | 4.32 | 25−60 | 0.00445−0.0181 |
| L-leucine | 9 | 9.77 | 25−60 | 0.00645−0.0224 |
| L-tyrosine | 5 | 2.50 | 30 | 0.000100−0.000350 |
| L-phenylalanine | 5 | 1.70 | 30 | 0.00189−0.00717 |
| L-lysine | 12 | 9.77 | 25−60 | 0.00645−0.0224 |
| L-histidine | 5 | 11.2 | 30 | 0.0101−0.0400 |
| L-arginine | 9 | 21.3 | 25−60 | 0.0608−0.173 |
| L-tryptophan | 16 | 4.64 | 25−60 | 0.00276−0.0110 |
| L-proline | 9 | 1.41 | 30−60 | 0.00286−0.00822 |
| L-asparagine | 5 | 1.16 | 30 | 0.00492−0.0300 |
| L-glutamine | 9 | 14.1 | 25−60 | 0.0142−0.0675 |

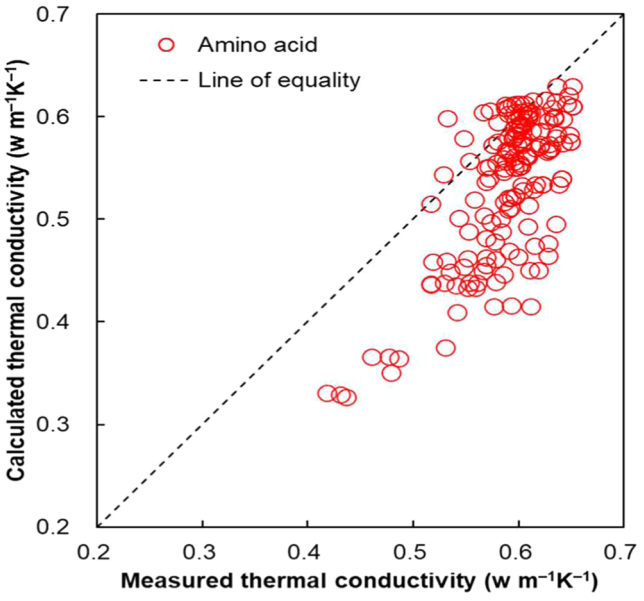


Figure 7. Experimental and calculated results of the thermal conductivity of amino acids in aqueous solutions.

0.00000553, 0.00900, and 0.0653, respectively. This indicates that the temperature did not affect the accuracy of the model.

**3.6. Overall Heat Transfer Coefficient Simulation.** In the simulation of the overall heat transfer coefficient, the reference values for density, heat capacity, viscosity, and thermal conductivity were calculated using a practical mixing rule model from a previous study.[1] This model demonstrated high accuracy because its mixing rule parameters were estimated based on actual experimental data. For aqueous L-valine solutions, MAPEs of the practical mixing rule model for the density, heat capacity, viscosity, and thermal conductivity were 0.0155, 0.0240, 0.880, and 0.722%, respectively. In contrast, the Python-based model used in this study did not use the mixing rule parameters, and MAPEs for the density,

Table 6. Simulation Results of Density, Heat Capacity, Viscosity, and Thermal Conductivity in a Commercial-Scale Falling Film Evaporator for L-Valine Production

| model | property | case 1 | case 2 | case 3 | case 4 |
|---|---|---|---|---|---|
| practical mixing rule model (reference) | density (kg $m^{-3}$) | 994 | 998 | 1005 | 1005 |
| | heat capacity (kJ $kg^{-1}$ $K^{-1}$) | 4.10 | 4.09 | 4.06 | 4.07 |
| | tube-side viscosity (cP) | 0.551 | 0.598 | 0.700 | 0.727 |
| | film viscosity (cP) | 0.546 | 0.592 | 0.687 | 0.719 |
| | thermal conductivity (W $m^{-1}$ $K^{-1}$) | 0.599 | 0.591 | 0.575 | 0.579 |
| Python-based model (this study) | density (kg $m^{-3}$) | 997 | 1001 | 1009 | 1009 |
| | heat capacity (kJ $kg^{-1}$ $K^{-1}$) | 4.04 | 4.02 | 3.98 | 4.00 |
| | tube-side viscosity (cP) | 0.415 | 0.441 | 0.492 | 0.533 |
| | film viscosity (cP) | 0.412 | 0.437 | 0.482 | 0.527 |
| | thermal conductivity (W $m^{-1}$ $K^{-1}$) | 0.405 | 0.395 | 0.377 | 0.393 |

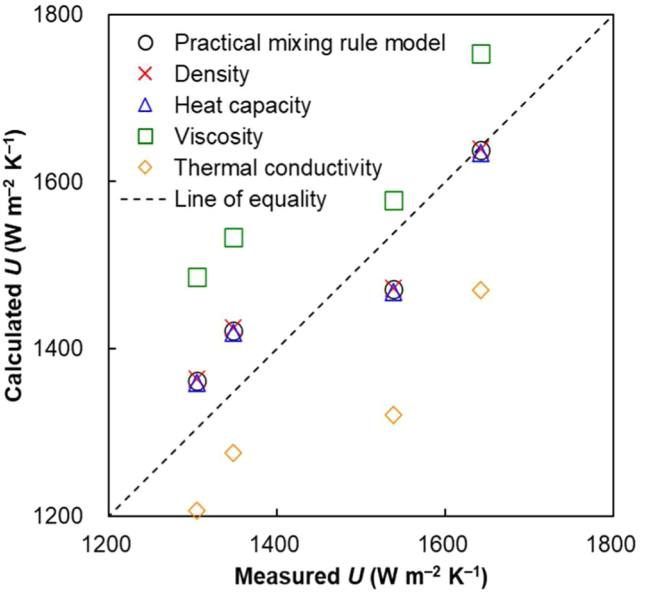


Figure 8. Measured and calculated overall heat transfer coefficients for the commercial-scale falling film evaporator used for L-valine production. The black circles represent the results of the practical mixing rule model (reference). The red crosses, blue triangles, green squares, and orange diamond symbols represent the results of replacing the values of the density, heat capacity, viscosity, and thermal conductivity with the values obtained from the Python-based model (this study), respectively.

heat capacity, viscosity, and thermal conductivity were 0.0349, 0.172, 10.6, and 16.3%, respectively.

Table 6 compares the results for the density, heat capacity, viscosity, and thermal conductivity of the four commercial-scale falling-film evaporators. The density and heat capacity values obtained from the Python-based model were similar to those obtained from the practical mixing rule model. However, the viscosity and thermal conductivity results of the Python-


https://doi.org/10.1021/acsomega.5c00424
ACS Omega 2025, 10, 16683−16694

based model were lower than those of the practical mixing rule model.

Figure 8 presents a comparison of the measured and calculated overall heat transfer coefficients. In the simulations, replacing the reference conditions, where the practical mixing rule parameters were applied, for the density or heat capacity with values obtained from the Python-based model did not result in any significant differences. MAPE for the overall heat transfer coefficient was 3.63% under the reference conditions. When the density and heat capacity simulations were replaced with values obtained from the Python-based model, MAPEs were 3.67 and 3.62%, respectively.

In contrast, replacing the viscosity value with that obtained from the Python-based model significantly increased the overall heat transfer coefficient, with the MAPE increasing to 9.27%. Similarly, replacing the thermal conductivity value with that obtained from the Python-based model caused a significant decrease in the overall heat transfer coefficient, resulting in a MAPE of 9.35%.

In summary, inaccurate physical property predictions can lead to significant changes in the heat exchanger calculations. If the overall heat transfer coefficient is overestimated in the simulations, it may result in an excessive initial investment costs. Conversely, underestimating the overall heat transfer coefficient may result in a unit process capacity that falls short of the design target. Therefore, it is recommended to consider the mixing rule parameters based on actual experimental data for estimating the solution properties during the process design phase of a commercial plant.

## 4. CONCLUSIONS

In this study, we developed a Python-based open-source algorithm that is compatible with the physical properties of aqueous mixtures provided in the electrolyte templates of AspenTech software. To verify the accuracy of the model, the results calculated using the proposed Python-based algorithm were compared with the experimental values of the properties of 37 binary aqueous mixture systems, including the density, heat capacity, viscosity, and thermal conductivity. MAPE for the density was 2.88%. However, the density of formic acid and acetic acid decreased as the concentration increased, which contrasted with the pattern observed for the other substances. MAPE for heat capacity was 0.355%. However, the model does not have the level of precision required to predict the temperature crossover point of the heat capacity of certain substances accurately. MAPE for viscosity was 12.1%. As the concentration of the aqueous solution increased, the calculated viscosities tended to be lower than the experimental values. Similarly, the MAPE for the thermal conductivity was 10.1%, and the calculated values tended to be lower than the experimental measurements as the concentration of the amino acid solutions increased.

The results of this study showed that parameter estimation using the Aspen PCES method, which is widely used in process simulations and serves as the basis for TEA (Technoeconomic Analysis) and LCA (Life Cycle Assessment), can lead to significant errors in the simulation of mixture properties. If experimental data are available, methods that use parameter regression can provide the most accurate results. Even in the absence of experimental data, molecular dynamics simulations can yield more accurate predictions of the density and viscosity of aqueous solutions. Nevertheless, this algorithm provides acceptable property values for substances that are not included in existing databases without the use of any commercial packages. In addition, this open-source software is fully compatible with the AspenTech software.

## ■ ASSOCIATED CONTENT

### Supporting Information

The Supporting Information is available free of charge at https://pubs.acs.org/doi/10.1021/acsomega.5c00424.

Summary of data for chemicals covered in this study (Table S1); experimental and calculated densities (Table S2); experimental and calculated heat capacities (Table S3); experimental and calculated viscosities (Table S4); experimental and calculated thermal conductivities (Table S5) (XLSX)

An in-house Python-based algorithm capable of calculating the properties of aqueous mixtures (ZIP)

## ■ AUTHOR INFORMATION


### Corresponding Authors

**Wangyun Won** − *Department of Chemical and Biological Engineering, Korea University, Seoul 02841, Republic of Korea;* orcid.org/0000-0003-1072-9842; Email: wwon@korea.ac.kr

**Jun-Woo Kim** − *CJ BIO Research Institute, CJ CheilJedang Corp., Suwon-si, Gyeonggi-do 16495, Republic of Korea;* orcid.org/0000-0002-2562-5491; Email: junwoo.kim1@cj.net

### Authors

**Jina Lee** − *CJ BIO Research Institute, CJ CheilJedang Corp., Suwon-si, Gyeonggi-do 16495, Republic of Korea;* orcid.org/0009-0002-8217-7039

**Se-Hee Jo** − *CJ BIO Research Institute, CJ CheilJedang Corp., Suwon-si, Gyeonggi-do 16495, Republic of Korea;* orcid.org/0009-0001-2799-2295

**Chungyup Lee** − *CJ BIO Research Institute, CJ CheilJedang Corp., Suwon-si, Gyeonggi-do 16495, Republic of Korea*

**Ji Hun Kang** − *CJ BIO Research Institute, CJ CheilJedang Corp., Suwon-si, Gyeonggi-do 16495, Republic of Korea*

Complete contact information is available at: https://pubs.acs.org/10.1021/acsomega.5c00424


### Notes

The authors declare no competing financial interest.

## ■ ACKNOWLEDGMENTS

This work is supported by the CJ BIO Research Institute, CJ CheilJedang, South Korea. Thanks to CJ CheilJedang for granting permission to publish this article. Professor Wangyun Won would like to acknowledge the financial support from the Industrial Strategic Technology Development Program (RS-2024-00432189, Development of Carbon-Reducing Consumer and Industrial Products Utilizing Vegetable Oil-based Bio-fine Chemical Materials) funded by the Ministry of Trade, Industry & Energy (MOTIE, Korea).

## ■ REFERENCES

(1) Kim, J.-W.; Lee, K. H.; Park, W. H.; Hong, S. B.; Park, C.; Kim, M.; Kim, J.-K. Development of thermophysical property models for aqueous amino acid solutions. *Chem. Eng. Technol.* **2023**, *46*, 702−710.

(2) Kim, J.-W.; Lee, K. H.; Park, W. H.; Lee, J.; Park, C.; Kim, M.; Kim, J.-K. Development of an Activity Coefficient Model for the Aqueous Amino Acid Solution. *Chem. Eng. Technol.* **2024**, *47*, 914−922.
(3) Lee, J.; Won, W.; Kim, J.-W. Python-Based Algorithm for Estimating the Parameters of Physical Property Models for Substances Not Available in Database. *ACS Omega* **2024**, *9*, 11895−11909.
(4) Ahn, B.; Jo, S.; Na, J.; Liu, J. J.; Kim, Y. J.; Won, W. Maximizing Biomass Utilization: An Integrated Strategy for Coproducing Multiple Chemicals. *J. Energy Chem.* **2025**, *100*, 180−191.
(5) Ferdous, J.; Bensebaa, F.; Pelletier, N. Integration of LCA, TEA, process simulation and optimization: A systematic review of current practices and scope to propose a framework for pulse processing pathways. *J. Cleaner Prod.* **2023**, *402*, No. 136804.
(6) Kwon, T.; Ahn, B.; Kang, K. H.; Won, W.; Ro, I. Unraveling the Role of Water in Mechanism Changes for Economically Viable Catalytic Plastic Upcycling. *Nat. Commun.* **2024**, *15*, No. 10239.
(7) Aspen physical property system. *Physical Property Methods and Models 11.1*, Aspentech 2001.
(8) Mashego, M. R.; Rumbold, K.; De Mey, M.; Vandamme, E.; Soetaert, W.; Heijnen, J. J. Microbial Metabolomics: Past, Present and Future Methodologies. *Biotechnol. Lett.* **2007**, *29*, 1−16.
(9) Kamal, K. M.; Maifiah, M. H. M.; Rahim, N. A.; Hashim, Y. Z. H. Y.; Sani, M. S. A.; Azizan, K. A. Bacterial Metabolomics: Sample Preparation Methods. *Biochem. Res. Int.* **2022**, *2022*, No. 9186536.
(10) Hanko, V. P.; Rohrer, J. S. Determination of Carbohydrates, Sugar Alcohols, and Glycols in Cell Cultures and Fermentation Broths Using High-Performance Anion-Exchange Chromatography with Pulsed Amperometric Detection. *Anal. Biochem.* **2000**, *283*, 192−199.
(11) Baaqel, H. A.; Bernardi, A.; Hallett, J. P.; Guillén-Gosálbez, G.; Chachuat, B. Global Sensitivity Analysis in Life-Cycle Assessment of Early-Stage Technology Using Detailed Process Simulation: Application to Dialkylimidazolium Ionic Liquid Production. *ACS Omega* **2023**, *11*, 7157−7169.
(12) Baaqel, H.; Díaz, I.; Tulus, V.; Chachuat, B.; Guillén-Gosálbez, G.; Hallett, J. P. Role of Life-Cycle Externalities in the Valuation of Protic Ionic Liquids—A Case Study in Biomass Pretreatment Solvents. *Green Chem.* **2020**, *22*, 3132−3140.
(13) Qian, Q.; Luo, Z.; Sun, H.; Wei, Q.; Shi, J.; Li, L. Life Cycle Assessment and Techno-Economic Analysis of Wood-Based Biorefineries for Cellulosic Ethanol Production. *Bioresour. Technol.* **2024**, *399*, No. 130595.
(14) Schemme, S.; Meschede, S.; Köller, M.; Samsun, R. C.; Peters, R.; Stolten, D. Property Data Estimation for Hemiformals, Methylene Glycols, and Polyoxymethylene Dimethyl Ethers and Process Optimization in Formaldehyde Synthesis. *Energies* **2020**, *13*, No. 3401.
(15) Pacheco, K. A.; Bresciani, A. E.; Nascimento, C. A.; Alves, R. M. Assessment of Property Estimation Methods for the Thermodynamics of Carbon Dioxide-Based Products. *Energy Convers. Manage.* **2020**, *211*, No. 112756.
(16) Yuan, X.; Ng, C. F.; Nikolic, H.; Liu, K. Linear Relationships for Modeling CO2 Absorption in Aqueous Alkanolamine Solutions in a Thermodynamically Consistent Way. *AIChE J.* **2022**, *68*, No. e17623.
(17) Hallamasek, S.; Ubbenjans, V.; Lapkin, A. A. Life Cycle Assessment of a Process for Paracetamol Flow Synthesis from Bio-Waste Derived $\beta$-Pinene. *Sustainable Chem. Pharm.* **2024**, *40*, No. 101629.
(18) Sharma, V. K.; Binder, T. P.; Allgeier, A. M. Conceptual Process Design and Techno-Economic Analysis of Biocatalytic Furfural Hydrogenation Using Ethanol as the Terminal Reductant. *ACS Sustainable Chem. Eng.* **2024**, *12*, 10776−10785.
(19) Brondani, L. B.; Flôres, G. B.; Soares, R. D. P. Modeling and simulation of a benzene recovery process by extractive distillation. *Braz. J. Chem. Eng.* **2015**, *32*, 283−291.
(20) Yang, Y.; Seo, K.; Kwon, J. S. I.; Won, W. Process Integration for the Production of Bioplastic Monomer: Techno-Economic Analysis and Life-Cycle Assessment. *ACS Sustainable Chem. Eng.* **2024**, *12*, 11167−11180.
(21) Kim, H.; Saremi, B.; Park, S.; Jung, M.; Yun, Y.; Son, J.; Lee, J.; Kim, J.-W.; Won, W. Comparative Life Cycle Assessment for the Sustainable Production of Fermentation-Based L-Methionine. *J. Cleaner Prod.* **2024**, *462*, No. 142700.
(22) Ahn, B.; Sohn, H.; Liu, J. J.; Won, W. A System-Level Analysis for Long-Distance Hydrogen Transport Using Liquid Organic Hydrogen Carriers (LOHCs): A Case Study in Australia−Korea. *ACS Sustainable Chem. Eng.* **2024**, *12*, 8630−8641.
(23) Park, D.; Lee, H.; Won, W. Unveiling the Environmental Gains of Biodegradable Plastics in the Waste Treatment Phase: A Cradle-to-Crave Life Cycle Assessment. *Chem. Eng. J.* **2024**, *487*, No. 150540.
(24) Pothakos, V.; Debeer, N.; Debonne, I.; Rodriguez, A.; Starr, J. N.; Anderson, T. Fermentation Titer Optimization and Impact on Energy and Water Consumption During Downstream Processing. *Chem. Eng. Technol.* **2018**, *41*, 2358−2365.
(25) Won, W.; Motagamwala, A. H.; Dumesic, J. A.; Maravelias, C. T. A Co-Solvent Hydrolysis Strategy for the Production of Biofuels: Process Synthesis and Technoeconomic Analysis. *React. Chem. Eng.* **2017**, *2*, 397−405.
(26) Chen, C. C.; Song, Y. Generalized Electrolyte-NRTL Model for Mixed-Solvent Electrolyte Systems. *AIChE J.* **2004**, *50*, 1928−1941.
(27) Jo, S.-H.; Lee, J.; Won, W.; Kim, J.-W. Python-Based Algorithm for Estimating NRTL Model Parameters with UNIFAC Model Simulation Results. *ACS Omega* **2025**, *10*, 2949−2957.
(28) Gunnell, L.; Nicholson, B.; Hedengren, J. D. Equation-based and data-driven modeling: Open-source software current state and future directions. *Comput. Chem. Eng.* **2024**, *181*, No. 108521.
(29) Wagner, W.; Pruß, A. The IAPWS Formulation 1995 for the Thermodynamic Properties of Ordinary Water Substance for General and Scientific Use. *J. Phys. Chem. Ref. Data* **2002**, *31*, 387−535.
(30) Rackett, H. G. Equation of state for saturated liquids. *J. Chem. Eng. Data* **1970**, *15*, 514−517.
(31) Hossain, N.; Bhattacharia, S. K.; Chen, C. C. Temperature Dependence of Interaction Parameters in Electrolyte NRTL Model. *AIChE J.* **2016**, *62*, 1244−1253.
(32) Que, H.; Chen, C. C. Thermodynamic Modeling of the $NH_3$−$CO_2$−$H_2O$ System with Electrolyte NRTL Model. *Ind. Eng. Chem. Res.* **2011**, *50*, 11406−11421.
(33) Que, H.; Song, Y.; Chen, C. C. Thermodynamic Modeling of the Sulfuric Acid−Water−Sulfur Trioxide System with the Symmetric Electrolyte NRTL Model. *J. Chem. Eng.* **2011**, *56*, 963−977.
(34) Fredenslund, A.; Jones, R. L.; Prausnitz, J. M. Group-Contribution Estimation of Activity Coefficients in Nonideal Liquid Mixtures. *AIChE J.* **1975**, *21*, 1086−1099.
(35) Kim, J.-W.; Park, W. H.; Park, C.; Rim, J. S.; Kim, G. H.; Jung, J. Y.; Kim, J.-K. Operational strategy of reconfigurable multi-effect evaporation processes for bio-based amino acid production. *Ind. Eng. Chem. Res.* **2024**, *63*, 12902−12915.
(36) Park, W. H.; Park, C.; Lee, J.; Choi, I.-J.; Kim, D.-H.; Kim, J.-W. Comparative analysis of multi-effect evaporators in an ammonium acetate concentration process for L-methionine production. *Sep. Purif. Technol.* **2025**, *354*, No. 128938.
(37) Jung, J. Y.; Kim, J.-W. Economic hybrid configuration of a multi-effect evaporative crystallizer for heat-sensitive L-glutamine with the simultaneous production of a heat-stable substance. *J. Food Eng.* **2025**, *391*, No. 112438.
(38) Kern, D. Q. *Process Heat Transfer*; McGraw-Hill: New York, 1950.
(39) Serth, R. W. *Process Heat Transfer Principles and Applications*; Academic Press: Burlington, 2007.
(40) Gunn, R. D.; Yamada, T. A corresponding states correlation of saturated liquid volumes. *AIChE J.* **1971**, *17*, 1341−1345.
(41) Germiniani, L. G. L.; Beppu, M. M.; Franco, L. F. Densities of the Standard Amino Acids in Aqueous Solutions via Molecular Dynamics Simulations. *J. Chem. Eng. Data* **2022**, *67*, 797−808.
(42) Deshchenya, V. I.; Kondratyuk, N. D.; Lankin, A. V.; Norman, G. E. Molecular Dynamics Study of Sucrose Aqueous Solutions: From


https://doi.org/10.1021/acsomega.5c00424
*ACS Omega* 2025, 10, 16683−16694

Solution Structure to Transport Coefficients. *J. Mol. Liq.* **2022**, *367*, No. 120456.
(43) Letsou, A.; Stiel, L. I. Viscosity of saturated nonpolar liquids at elevated pressures. *AIChE J.* **1973**, *19*, 409−411.
(44) Andrews, C. T.; Elcock, A. H. Molecular Dynamics Simulations of Highly Crowded Amino Acid Solutions: Comparisons of Eight Different Force Field Combinations with Experiment and with Each Other. *J. Chem. Theory Comput.* **2013**, *9*, 4585−4602.



https://doi.org/10.1021/acsomega.5c00424
*ACS Omega* 2025, 10, 16683−16694